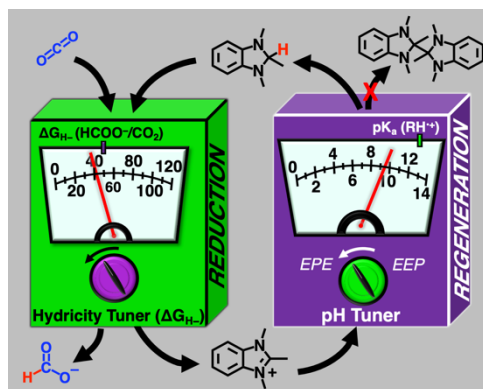


Biomimetic Metal-free Hydride Donor Catalysts for CO₂ Reduction

Stefan Ilic,^{1,2} Jonathan L Gesiorski,¹ Ravindra B Weerasooriya,^{1,2} and Ksenija D Glusac*^{1,2}

¹Department of Chemistry, University of Illinois at Chicago, 845 W Taylor Street, Chicago, Illinois 60607, United States

²Chemical Sciences and Engineering Division, Argonne National Laboratory, 9700 Cass Ave, Lemont, Illinois, 60439, United States



Conspectus

Catalytic reduction of carbon dioxide to fuels and value-added chemicals is of significance for the development of carbon recycling technologies. One of the main challenges associated with catalytic CO₂ reduction is product selectivity: the formation of carbon monoxide, molecular hydrogen, formate, methanol, and other products occur with similar thermodynamic driving forces, making it difficult to selectively reduce CO₂ to the target product. Significant scientific effort has been aimed at the development of catalysts that can suppress the undesired hydrogen evolution reaction and direct the reaction toward selective formation of the desired products, that are easy to handle and store. Inspired by natural photosynthesis, where the CO₂ reduction is achieved using NADPH cofactors in the Calvin cycle, we explore biomimetic metal-free hydride donors as catalysts for the selective reduction of CO₂ to formate. Here, we outline our recent findings on the thermodynamic and kinetic parameters that control the hydride transfer from metal-free hydrides to CO₂. By experimentally measuring and theoretically calculating thermodynamic hydricities of a range of metal-free hydride donors, we derive structural and electronic factors that affect their hydride-donating abilities. Two dominant factors that contribute to the stronger hydride donors are identified to be: i) the stabilization of the positive charge formed upon HT via aromatization or by presence of electron-donating groups; and (ii) destabilization of hydride donors through anomeric effect or presence of significant structural constraints in the hydride molecule. Hydride donors with appropriate thermodynamic hydricities were reacted with CO₂ and the formation of the formate ion (the first reduction step in CO₂ reduction to methanol) was confirmed experimentally, providing an important proof-of-principle that organocatalytic CO₂ reduction is feasible. The kinetics of hydride transfer to CO₂ were found to be slow, and the sluggish kinetics were assigned

in part to the large self-exchange reorganization energy associated with the organic hydrides in the DMSO solvent. Finally, we outline our approaches toward the closure of the catalytic cycle via electrochemical and photochemical regeneration of the hydride (R–H) from the conjugate hydride acceptors (R⁺). We illustrate how proton-coupled electron transfer can be efficiently utilized, not only to lower the electrochemical potential at which the hydride regeneration takes place, but also to suppress the unwanted dimerization that neutral radical intermediates tend to undergo. Overall, this account provides a summary of important milestones achieved in organocatalytic CO₂ reduction and provides insights into the future research directions needed for the discovery of inexpensive catalysts for carbon recycling.

Key References

Ilic, S.; Kadel, U. P.; Basdogan, Y.; Keith, J. A.; Glusac, K. D. Thermodynamic Hydricities of Biomimetic Organic Hydride Donors. *J. Am. Chem. Soc.* **2018**, 140, 4569–4579¹ *The study investigates thermodynamic hydricities of metal-free hydride donors. Electronic and structural factors, such as aromatization, charge delocalization of the conjugate hydride acceptor, and hyperconjugation, were identified as parameters that contribute to the hydride ion release.*

Lim, C. H.; Ilic, S.; Alherz, A.; Worrell, B. T.; Bacon, S. S.; Hynes, J. T.; Glusac, K. D.; Musgrave, C. B. Benzimidazoles as Metal-Free and Recyclable Hydrides for CO₂ Reduction to Formate. *J. Am. Chem. Soc.* **2019**, 141, 272–280² *The study demonstrates that the reduction of CO₂ to formate can be achieved by a hydride transfer from benzimidazole-based hydride donors. The formate formation has been quantified and the electrochemical recycling of the hydride demonstrated.*

Weerasooriya, R. B.; Gesiorski, J. L.; Alherz, A.; Ilic, S.; Hargenrader, G. N.; Musgrave, C. B.; Glusac, K. D. Kinetics of Hydride Transfer from Catalytic Metal-Free Hydride Donors to CO₂. *J. Phys. Chem. Lett.* **2021**, 12, 2306–2311³ *The study investigates the kinetic aspects of hydride transfer from organic hydrides to CO₂. The Marcus formalism shows that the reaction kinetics are sluggish due to the large self-exchange reorganization energy associated with the organic hydride donors.*

Ilic, S.; Alherz, A.; Musgrave, C. B.; Glusac, K. D. Importance of Proton-Coupled Electron Transfer in Cathodic Regeneration of Organic Hydrides. *Chem. Commun.*, **2019**, 55, 5583–5586⁴ *The study explores proton-coupled electron transfer in the electrochemical reduction of conjugate hydride acceptors to the corresponding hydride donors. When the pKa values of the relevant radical cations are appropriate, the proton-coupled mechanism was shown to lower the electrochemical potential.*

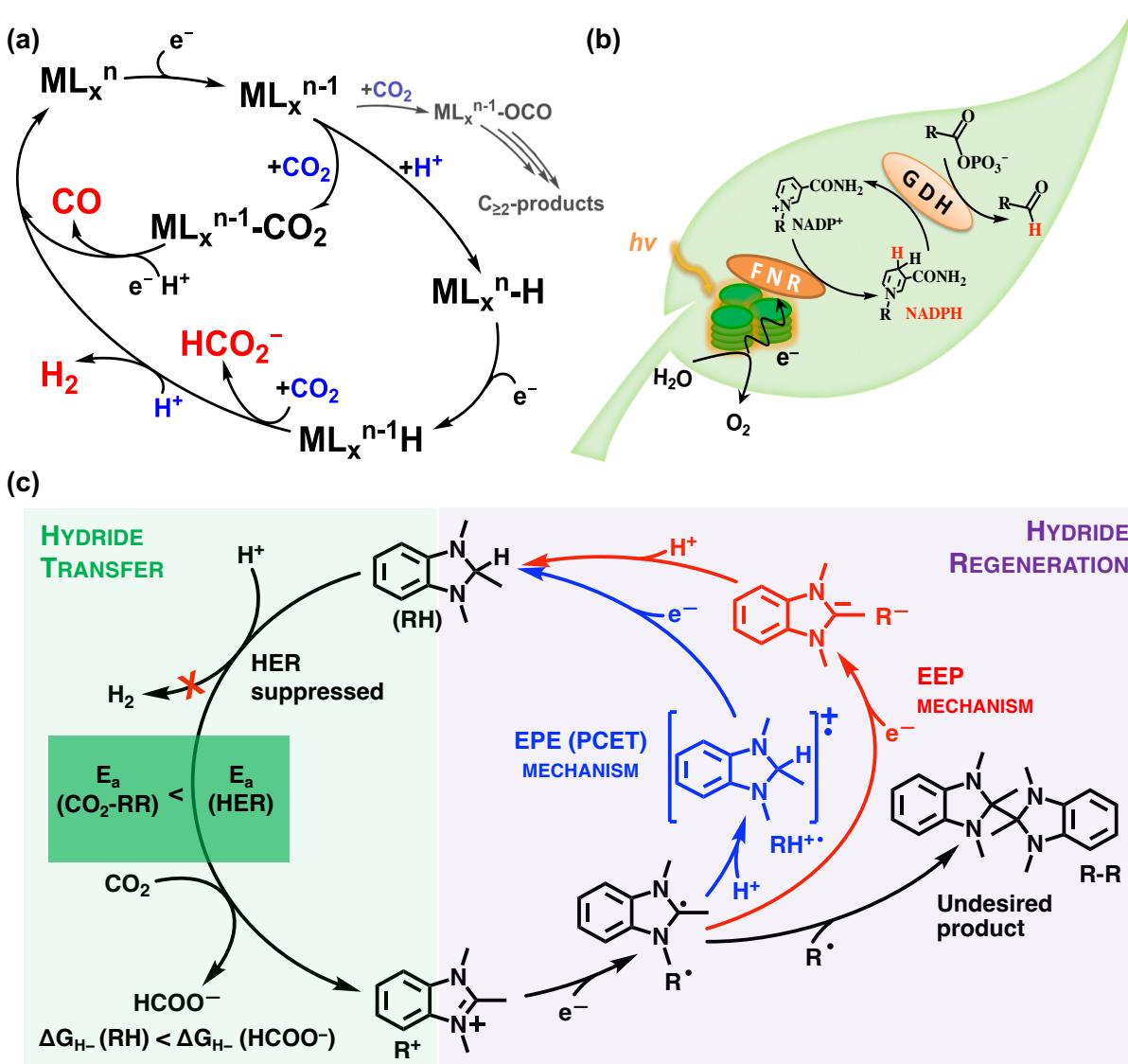
Introduction

The conversion of carbon dioxide to value-added chemicals (e.g. polycarbonates) and fuels (e. g. methanol) is of increasing scientific interest, driven by the need to slow down the climate change caused by human-induced carbon dioxide emissions.^{5,6} Some of the target chemical transformations for CO₂ utilization require a relatively small energy input and generally do not change the oxidation state of the carbon center. One such transformation involves the production of urea from CO₂ and NH₃, a mature technology currently used to produce 155 Mt/year of urea for

agricultural fertilizers and other products.⁷ However, urea production would need to increase ~200 times more urea production to compensate the current anthropogenic carbon input. In contrast, the reductive transformations that generate carbon with lower oxidation state, such as +2 (formic acid), 0 (formaldehyde) or -2 (methanol), are more energy intensive and challenging. The products obtained from these transformations can serve as fuels to generate electricity or heat. The reductive CO₂ conversion can be achieved chemically, via thermal hydrogenation reaction, or electrochemically/photochemically, using water as a terminal proton and electron source. While thermal methods are at a higher technology readiness level, with several methanol-producing plants via CO₂ hydrogenation currently under operation,⁸ the electrochemical and photochemical methods are more advantageous, because they are more readily coupled to renewable sources of energy, such as solar and wind. Furthermore, theoretical thermal efficiencies of electrochemical methods are higher (can reach unity for an ideal cell) than those achievable by thermal methods (ideal efficiency can be up to $1 - T_C/T_H$, where T_C is the absolute temperature of the cold reservoir and T_H is the absolute temperature of the hot reservoir, as known from the Carnot cycle). The losses in thermal processes are associated with the incompleteness of any heat transfer process that occurs at temperatures that are not absolute zero. The electrochemical methods rely on charge transfer processes, where all energy of an electron can be used up, if resistance losses and overpotentials are negligible.⁹

Extensive mechanistic studies have been performed on transition-metal based molecular electrocatalysts for CO₂ reduction, providing information regarding the factors that control catalytic rates, overpotentials and product selectivity.^{10–12} In general, the catalytic cycle is initiated by the metal-centered reduction, which is often coupled with the loss of a labile ligand (Scheme 1a). The reduced transition metal complex becomes sufficiently nucleophilic to react either with CO₂ to form the metal-carboxylate intermediate or with protons to form the metal hydride. The relative rates of these two reactions dictate the product selectivity: metal-carboxylate intermediates lead to the reduction of carbon dioxide to CO and C₂₊-products, while metal hydride intermediates direct the reactivity towards proton reduction and hydride transfer products, like formate and methanol. Careful control of thermodynamic parameters, such as the pKa value of the proton donor, can be used to steer the reactivity in the desired direction.¹³ The metal carboxylate intermediate M-CO₂ is usually a precursor for CO formation, while its M-OCO isomer is responsible for the formation of oxalate and beyond products.¹⁴ The selective stabilization of one of the two carboxylate and hydride intermediates can be achieved using a proper choice of the metal-ligand couple.^{10,15} Overall, homogeneous transition-metal based catalysts often catalyze the reduction of CO₂ to CO,^{16–22} less frequently the reduction to formate,^{13,23–28} and very rarely to methanol.^{29,30} While more recent reports show how you can thermodynamically navigate toward formate formation,^{31–34} there is still a need for a discovery of new catalysts that are more efficient in suppressing the hydrogen evolution reaction.

Scheme 1. Catalytic CO₂ reduction by: (a) Transition metal-complexes; (b) NADPH cofactor in natural photosynthesis; and (c) Biomimetic NADPH analogs. The catalytic cycle is divided into the hydride transfer (green) and hydride regeneration (purple) steps.



In natural photosynthesis, plants and other organisms convert CO_2 to energetically dense molecules using sunlight as an energy input. This process depends on a variety of cofactors including, nicotinamide adenine dinucleotide phosphate (NADPH), which is responsible for the reduction of “captured” CO_2 via a hydride transfer (HT) mechanism (Scheme 1b). Specifically, CO_2 is captured within the Calvin cycle to generate 1,3-bisphosphoglycerate, which is then reduced via HT from NADPH to generate glyceraldehyde-3-phosphate, a key precursor in the self-synthesis of biomass and other energy-dense molecules (glucose).³⁵ The oxidized NADP^+ cofactor is then reduced back to the hydride form using the sunlight as an energy source and water as an electron/proton source. Thus, the overall photocatalytic transformation is achieved by an organic reduction catalyst, NADPH. Photosynthesis demonstrates that plants can selectively synthesize the molecules necessary for their growth using the resources available around them, such as ambient CO_2 , which comprises $\sim 0.04\%$ of our atmospheric gases,³⁶ and earth-abundant CO_2 reduction organocatalysts.

Herein, we present our exploration of biomimetic NAPDH analogs as potential electro- and photocatalysts for the selective reduction of CO₂ to formate. Our work is motivated by the scalability and low cost of such earth-abundant organocatalytic systems. Furthermore, the HT mechanism is critical for the selective formation of formate, a product that is rarely formed when metal-based catalysts are used, thus, avoiding the formation of CO. The overall catalytic cycle under investigation is shown in Scheme 1 and is divided into the HT and hydride regeneration steps. We first present the results of our work involving the HT step, by discussing thermodynamic hydricities of a series of carbon-based hydride donors (R-H) and their reactivity with CO₂. These studies provide insights into structure-property relationships that control the hydricities of R-H derivatives, as well as kinetics barriers associated with the HT process. The second section of this report reviews our hydride regeneration approaches. We show how the proton-coupled electron transfer (PCET) mechanism can be utilized to lower the overpotential for electrochemical reduction of R⁺ derivatives and to prevent undesired dimerization of one-electron reduced R[•] radical. We also show our studies of photochemical regeneration of R-H derivatives using wide and mid-gap inorganic semiconductor photoelectrodes. Overall, our work provides important proof-of-principle demonstrations of successful metal-free (photo)electrocatalysis involving R-H donors. Furthermore, our work points out the challenges that still need to be addressed to enable fast and energy-efficient CO₂ reduction catalysis by NADPH analogs.

Hydride Transfer to CO₂

Thermodynamics. Metal-free hydrides, just like metal-based analogs, differ in their hydride donor ability based on their structural and electronic characteristics. To establish design strategies that contribute to stronger hydrides, thermodynamic parameters that describe their hydride donor ability need to be considered. For that purpose, the most readily applicable descriptor with the largest available database is thermodynamic hydricity (ΔG_{H^-}), defined as the standard Gibbs free energy required for the hydride ion release:



Given that a high-energy intermediate, the hydride ion, is released, reaction (1) is never spontaneous and ΔG_{H^-} values are always positive numbers. A lower ΔG_{H^-} value indicates a stronger hydride (for example, ΔG_{H^-} for LiAlH₄ is 43 kcal/mol in acetonitrile³⁷) while higher ΔG_{H^-} value indicates weaker hydride donors (for example, ΔG_{H^-} for NaBH₄ is 50 kcal/mol in acetonitrile³⁷). The ΔG_{H^-} values serve as excellent markers for the donor's HT abilities, decoupled from the nature of the hydride acceptor.

Despite many experimental hydricities reported for metal-based hydrides,^{23,24,38-44} only a handful of stronger metal-free hydrides have been experimentally evaluated.⁴⁵⁻⁴⁸ This trend is not consistent with experimental challenges associated with metal-based hydride donors: interactions of solvent and anion molecules with the metal-based conjugate hydride acceptor are known to affect the observed hydricities.^{49,50} Such interactions do not affect metal-free hydride donors, making them easier to study. Our group and others have utilized commonly used “potential-pKa”

and “hydride transfer” methods, both based on thermochemical cycles,³¹ to determine the ΔG_{H^-} values of metal-free hydride donors (Scheme 2). The “potential-pK_a” method utilizes a thermodynamic cycle that involves equations 2a–d. In this approach, the ΔG values for 2a–c are obtained from the pK_a values of R-H derivatives (using spectrophotometric titration) and the experimentally-obtained standard reduction potentials for R⁺/R[•] and R[•]/R⁻ couples (using cyclic voltammetry) and the pK_a values of R-H derivatives (using spectrophotometric titration). The ΔG value for 2d is obtained from the standard reduction potential for the H⁺/H⁻ couple. Given that this reduction potential is not directly available in nonaqueous solvents, several assumptions (mostly regarding solvation) were employed to derive the $\Delta G_{H^+/H^-}$ value of 69.9 kcal/mol and 54.7 kcal/mol in DMSO and ACN, respectively.⁵¹ The “potential-pK_a” method has been utilized to obtain thermodynamic hydricities of weak hydrides while the thermodynamic hydricity of stronger hydrides are more commonly determined using the “hydride transfer” method (eq 3a–b). In this method, the ΔG_{H^-} values are derived from ΔG_{HT} (equation 3a), obtained from the equilibrium constant for HT between a donor of interest R-H and a reference hydride acceptor A⁺ with known hydride affinity, (expressed as the negative of the hydricity of A-H, equation (3b)). hydricity ($\Delta G_{HT}(AH)$). For the ΔG_{HT} to be experimentally measurable, the difference in hydricity between R-H and A-H needs to be in the ± 2 –3 kcal/mol range. As such, the method may require several hydride acceptors A⁺ to be tested before the appropriate reference is established. Experimentally less challenging is to determine the enthalpic hydricity ΔH_{H^-} by measuring the heat change for the hydride transfer reaction via calorimetry. However, the corresponding entropic contributions need to be negligible or consistent in order to use ΔH_{H^-} values to characterize a wide range of hydrides. Since this is not the case,⁵² the ΔH_{H^-} values can be used only to compare structurally similar hydride donors.

Scheme 2. Thermochemical cycles used to experimentally determine the ΔG_{H_2} values.

<u>"potential-pK_a" method</u>		<u>"hydride transfer" method</u>	
$RH \rightarrow R^- + H^+$	$\Delta G = 1.364 \text{ p}K_a^{RH}$	$RH + A^+ \rightarrow R^+ + AH$	$\Delta G = -1.364 \log(K_{eq})$
$R^- \rightarrow R^+ + e^-$	$\Delta G = 23.06 E_{R^+/R^-}^0$	$AH \rightarrow AH + H^-$	$\Delta G_{H-}(AH)$
$R^+ \rightarrow R^+ + e^-$	$\Delta G = 23.06 E_{R^+/R^+}^0$	$RH \rightarrow R^+ + H^-$	$\Delta G_{H-}(RH)$
$H^+ + 2e^- \rightarrow H^-$	$\Delta G_{DMSO/ACN}^{H^+/H^-}$		
$RH \rightarrow R^+ + H^-$	$\Delta G_{H-}(RH)$		

Given the challenges associated with the experimental ΔG_{H^-} determination,⁵² computational evaluation represents a more straightforward and easier alternative. The computational approach involves calculations of absolute Gibbs free energies for solvated species in equation 1. While $G_{\text{R}-\text{H}}$ and $G_{\text{R}+}$ can be accurately calculated with commonly used implicit solvent models, the computational treatment of the solvated H^+ ion is far less trivial. Namely, the available solvation models fail to account for the interactions between the solvated hydride ion and solvent molecules, such as dispersion, repulsion, and hydrogen-bonding. Instead, the calculation of absolute Gibbs free energies for the solvated hydride ion can be successfully circumvented by using the linear scaling approach, where G_{H^-} is extracted from the correlation between the experimental hydricity values and calculated $G_{\text{R}-\text{H}}$ and $G_{\text{R}+}$ (eq 1).⁵² Alternatively, the solvated G_{H^-} can be obtained from the calculation of G_{H^-} in the gas-phase by adding the experimental correction for solvation effects.^{1,53} Our previous studies indicated that the calculated hydricity values are in reasonably

good agreement with the experimental results (within 3 kcal/mol),^{1,52} which enables screening of a wide range of metal-free hydride donors, even those that have yet to be synthesized.

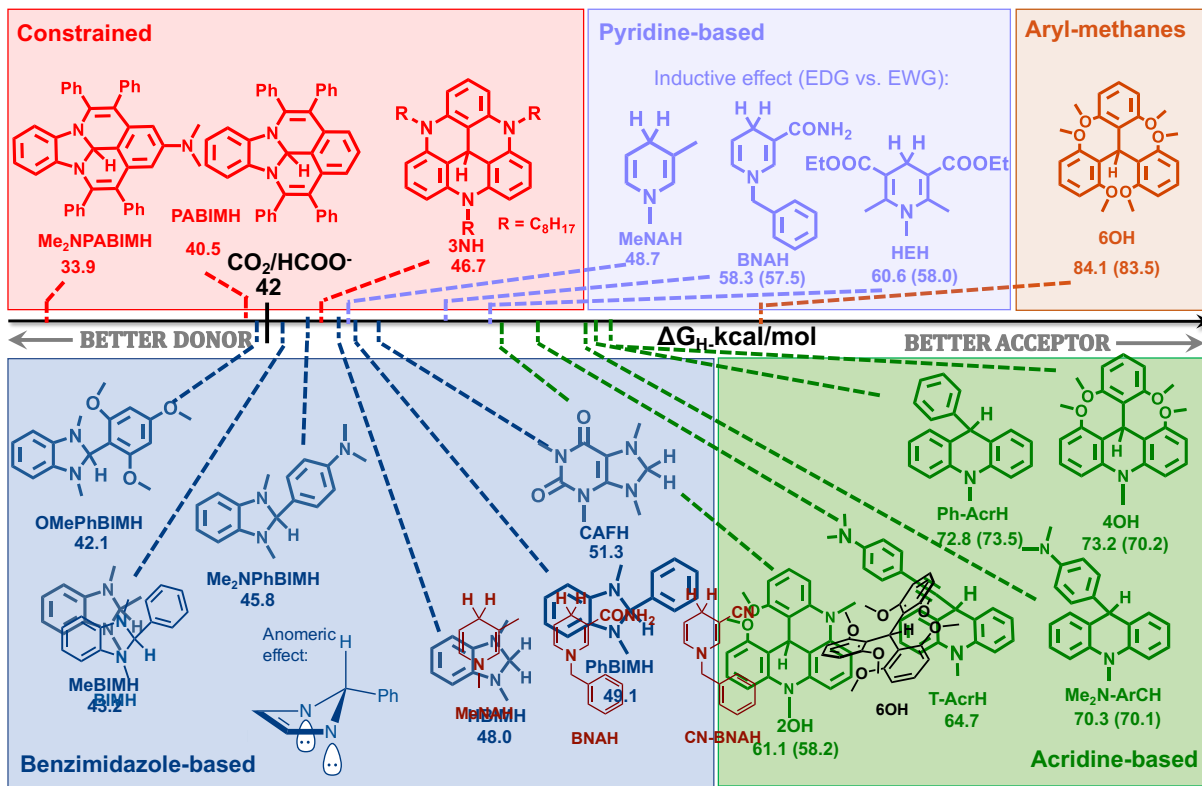


Figure 1. Calculated and experimental (in parentheses) thermodynamic hydricities for selected hydrides in DMSO. Data taken from refs. ^{1,3,38}

For the HT reaction between hydride donor R-H and the acceptor A⁺ to take place spontaneously, the donor needs to have a lower ΔG_{H-} value than the hydricity of the conjugate acceptor A-H. For example, Figure 1 compares ΔG_{H-} values of metal-free hydride donors investigated in our lab, along with the hydricities of molecular hydrogen and the formate ion. This comparison shows that, based on thermodynamic arguments, any donor with ΔG_{H-} values lower than 60.7 kcal/mol can reduce protons to H₂ in DMSO. However, the reduction of CO₂ to formate is more challenging and requires R-H donors with hydricities that are lower than 42.0 kcal/mol. Two structural arguments that contribute to stronger hydrides are: (i) the ability to stabilize the positive charge formed on R⁺ species after HT and (ii) the factors that lead to relative destabilization of the donor R-H. In metal-free systems, the positive charge is stabilized through either extended delocalization or aromatization mechanisms. Aromatization upon HT is an efficient method to stabilize the positive charge formed and yields relatively strong hydrides. In fact, aromatization is the main driving force for hydride release from many biologically relevant cofactors, such as NADH,^{54,55} FADH₂,⁵⁵ and H4MPT.^{52,56} The positive charge on R⁺ can be further stabilized through the inductive effect, achieved in the presence of electron-donating groups (such as amines, alcohols, etc.). For example, Figure 1 shows that ΔG_{H-} values decrease in the HEH > BNAH > MeNAH series, illustrating the effect of increasing inductance with increasingly donating groups.

The relative destabilization of R-H also leads to improved hydricities. For example, the weakening of the R-H bond through the so-called anomeric effect^{57,58} has been used to explain the lower ΔG_{H^-} values of benzimidazole-based derivatives (X-BIMH, Figure 1). Here, the hyperconjugation involving the donation of the lone pairs of electrons from the neighboring nitrogen atoms into the σ^* orbital of the C-H bond leads to the weakening of the C-H bond and thus, the improved hydride donating ability of R-H. In addition, the hydride R-H can be destabilized via significant structural strain, where the hydride ion removal results in a release of strain. Such behavior is exemplified with compounds 3NH, PABIMH and Me₂NPABIMH, where the extended conjugation imposes a tendency of the molecule to adopt a planar conformation, imposing strain onto the sp³ hybridized hydridic C-H bond in the compound. Combined, these electronic and structural factors can tune thermodynamic hydricities of carbon-based hydride donors within the 30–90 kcal/mol range, enabling applications in many HT processes. Hydrides in Figure 1 can be classified into three structural groups with characteristic hydride donor abilities. First, arylmethanes are relatively weak hydrides ($\Delta G_{H^-} = 75$ –90 kcal/mol) and are not relevant for CO₂ reduction. Next, pyridine- and acridine-based hydrides display significantly improved hydride donor ability (46–76 kcal/mol), which is achieved via R⁺ aromatization upon hydride loss. These hydrides have already been employed in synthetic transformations as stoichiometric reducing reagents.^{59–65} Strong hydride donors (with $\Delta G_{H^-} < 40$ kcal/mol) are the most applicable for HT to CO₂ and the reactivities of these derivatives with CO₂ has been further explored.

Given that the hydricities of benzimidazoles are similar or even lower than that of formate ($\Delta G_{H^-} = 42$ kcal/mol), these hydrides represent suitable candidates for CO₂ reduction reactions. Indeed, benzimidazoles in Figure 2 were the first carbon-based hydrides reported to selectively reduce CO₂ to formate.² The experimentally observed reactivity correlates with the calculated free energies for HT, ΔG_{HT} (Figure 2). The highest formate yield (66%, Figure 2) was achieved using MeBIMH in the presence of KBF₄ in DMSO under mild conditions. The addition of exogenous salts stabilizes charged products, such as R⁺ and HCOO[–], by increasing the ionic strength of the medium. Similarly, the HT reaction was found to be solvent dependent, where more polar solvents resulted in higher yields due to the same effect on product stabilization. This study served as a proof of principle that selective CO₂ reduction can be carried out using carbon-based hydride donors.

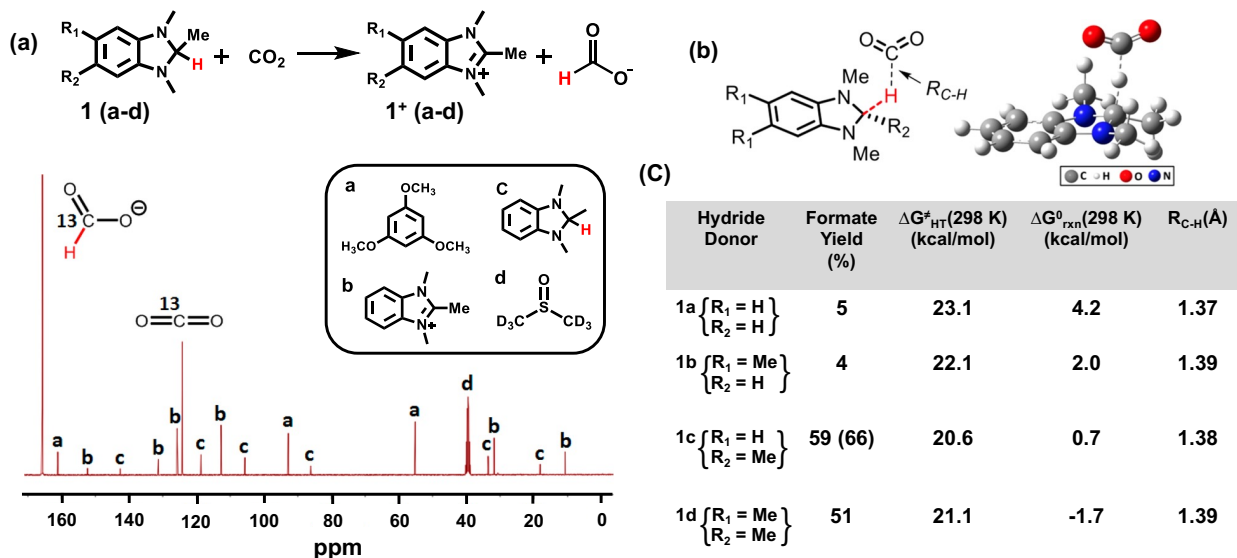


Figure 2. The reduction of CO_2 to formate using organic hydrides: (a) ^{13}C NMR spectra of the reaction between MeBIMH and $^{13}\text{CO}_2$ in DMSO-d_6 ; (b) HT transition state structure calculated at the RM06/6-31+G(d,p) level of theory; (c) Calculated ΔG^0_{HT} and $\Delta G^{\ddagger}_{\text{HT}}$ values for HT, along with the calculated C-H bond lengths in the transition state. Reproduced with permission from ref 2. Copyright 2019 American Chemical Society.

The HT reactivity could certainly be further improved by using stronger hydride donors. However, as is always the case in catalysis, the improved reactivity of R-H would come at the expense of an increase in energy needed to regenerate the reduced form of the catalyst from R^+ . This correlation is best observed in Figure 3, which plots $\Delta G_{\text{H-}}$ values of R-H as a function of the standard reduction potential for the $\text{R}^+/\text{R}^\bullet$ couple.⁵² The presence of a linear dependence is a clear indication that the scaling relationship exists between the two parameters, making it difficult to improve HT reactivity without introducing an overpotential in the catalyst regeneration step. Figure 3 also shows a point where an ideal catalyst for the reduction of CO_2 to formate should be, based on the standard reduction potential for $\text{CO}_2/\text{HCOO}^-$ couple (-0.23 V vs NHE) and the hydricity of formate (42 kcal/mol). It is obvious from Figure 3 that none of the metal-free derivatives R-H exhibit desired hydricity/reduction potential values and that a significant overpotential is expected in metal-free CO_2 reduction to formate (~1.5 V). Similarly, metal-based hydride donor exhibit a scaling relationship between $\Delta G_{\text{H-}}$ and $E^\circ(\text{M}^{\text{n}+}/\text{M}^{(\text{n}-1)+})$ values, albeit, with smaller overpotentials due to the lower bond dissociation energy of the M-H bond.⁵²

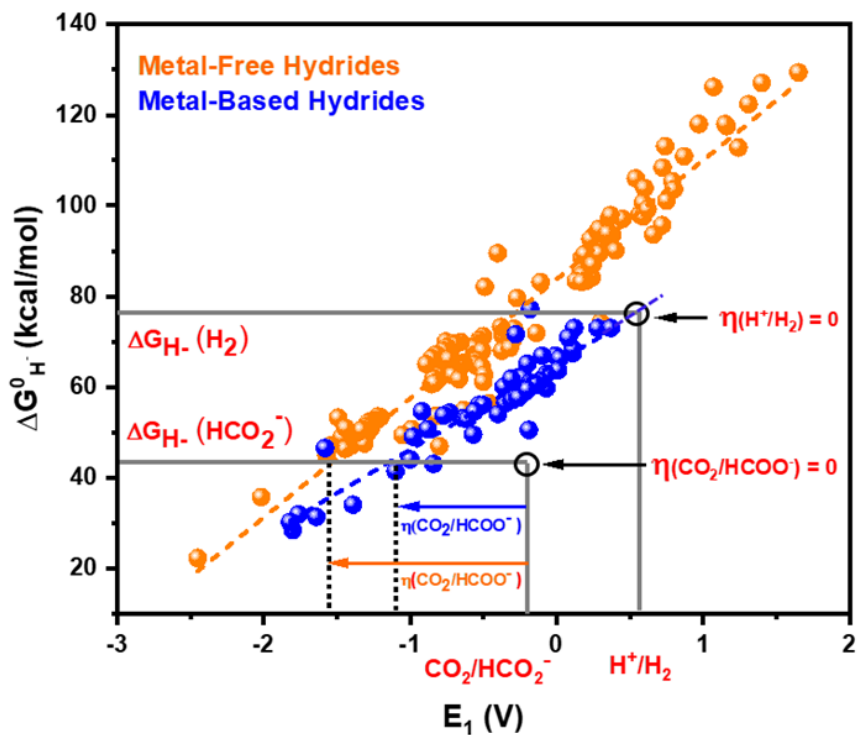


Figure 3: Scaling relationship between the thermodynamic hydricity ΔG_{H^-} and the first electron reduction potential E_1 (vs. NHE) of R^+ for metal-free (orange) and metal-based hydrides (blue) in acetonitrile. The dashed lines indicate the estimated overpotential for CO_2 reduction catalysis. Reproduced with permission from ref 46. Copyright 2018 Royal Society of Chemistry.

Kinetics. To further explore the origins of the sluggish reactivity observed in Figure 2, we investigated the HT kinetics from a series of organic hydrides to CO_2 .³ Several experimental conditions were explored to maximize formate production via CO_2 reduction by organo-hydrides. Namely, the highest formate yield (70%) was achieved at 100°C, at a mild CO_2 pressure of ~2.2 atm and in the presence of 20 eq of KBF_4 in DMSO. Temperature-dependent studies were performed using the optimized reaction conditions in the temperature range of 70–100°C for the reaction. The HT reactions were monitored using 1H NMR spectroscopy (Figure 4a) and the observed changes in the reactant/product concentrations were modeled using kinetic equations derived from rate laws for two possible HT reactions (Figure 4b and c) at several temperatures (Figure 4c) to determine free energy barriers (ΔG^\ddagger) for:



The experimental free energy barrier for the HT to CO_2 were found to be range in $\Delta G^\ddagger = 15-21$ kcal/mol for the reactions with thermodynamic driving forces in the $\Delta G_{rxn} = -11-5$ kcal/mol range.

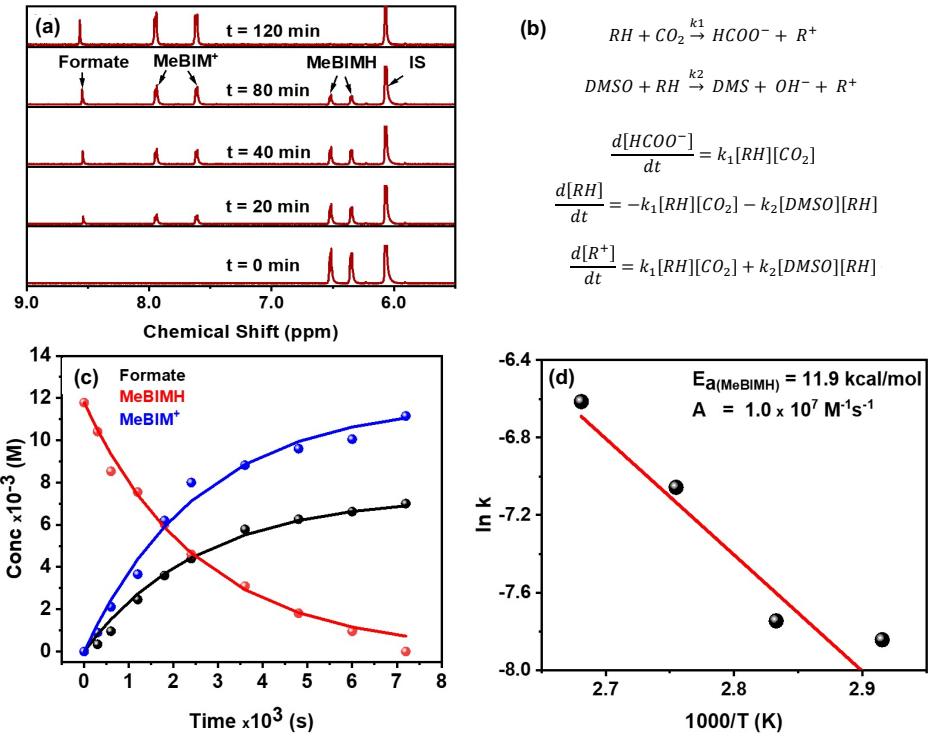


Figure 4. Kinetic studies of the HT reaction from MeBIMH to CO₂ in DMSO-d₆: (a) Time dependent ¹H-NMR spectral characterization for the reaction of MeBIMH and CO₂, (b) two possible hydride transfer reactions – to CO₂, and solvent (DMSO); (c) change in concentrations of reactants and products as a function of time for the HT (solid lines represent fits of the kinetic model) and (c) Arrhenius plot for the HT reaction obtained from temperature-depended kinetic experiments. Reproduced with permission from ref 3. Copyright 2021 American Chemical Society.

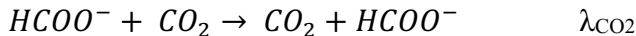
The Marcus formalism was applied to explore the correlation between the free energy barrier (ΔG^\ddagger) and thermodynamic driving force (ΔG^0) for HT to CO₂. The goal of this study was to evaluate the reorganization energy associated with HT to CO₂. According to Marcus theory, the activation free energy barrier can be expressed as:

$$\Delta G^\ddagger = W_r + \frac{\lambda}{4} + \frac{\Delta G^{0\prime}}{2} + \frac{(\Delta G^{0\prime})^2}{4\lambda} \quad (5)$$

where W_r is the free energy required for the formation of precursor complex and ($\Delta G^{0\prime}$) is the thermodynamic driving force of the reaction, corrected for the free energy of the encounter complex. The reorganization energy λ is the energy associated with the reorganization of the nuclei and the solvent upon the hydride transfer and is assumed to be independent of the structure of the hydride donor. The experimental value was found to be $\lambda = 74 \text{ kcal/mol}$ and was consistent with value of $\lambda = 70 \text{ kcal/mol}$ obtained using DFT calculations. This reorganization energy was further partitioned into contributions from the hydride donor, RH, and from the hydride acceptor, CO₂, using the corresponding self-exchange reorganization energies λ_{RH} and λ_{CO_2} , as follows:

$$\lambda = \frac{\lambda_{RH} + \lambda_{CO_2}}{2} \quad (6)$$

$$RH + R^+ \rightarrow R^+ + RH \quad \lambda_{RH}$$



Self-exchange reorganization energies obtained using this approach were found to be quite high: $\lambda_{RH} = 98$ kcal/mol and $\lambda_{CO_2} = 49$ kcal/mol. The large $\lambda_{CO_2} = 49$ kcal/mol is most likely associated with the significant structural distortion associated with the conversion of the linear reactant, CO_2 , to the bent δ formate ion. Similar arguments were used to explain the large self-exchange reorganization energy associated with the electron transfer to CO_2 to form CO_2^- radical anion.⁶⁶ The large λ_{RH} value shows that organic hydrides undergo significant structural rearrangement upon HT, and this reorganization is likely associated with the planarization of R^+ .

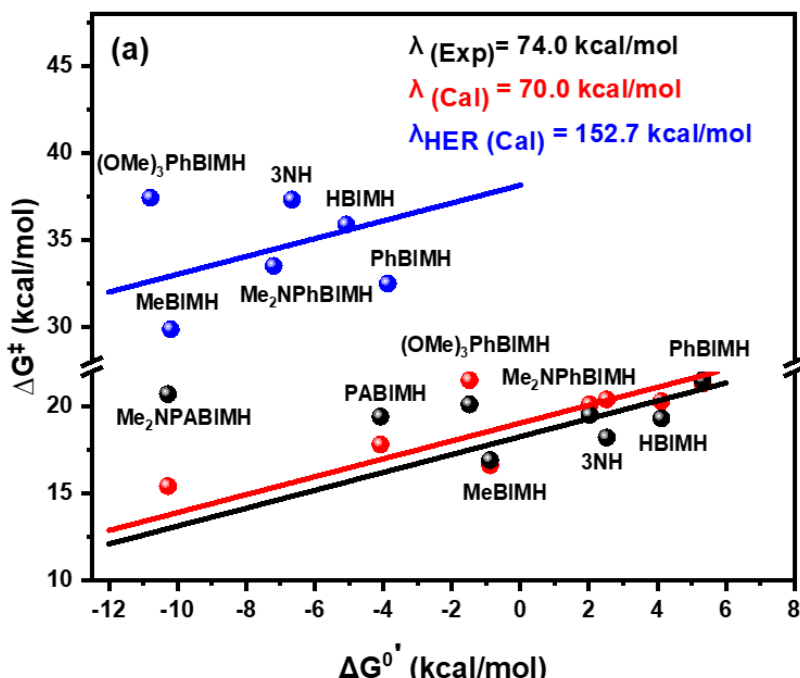


Figure 5. The correlation between free energy barriers (ΔG^\ddagger) and reaction free energies ($\Delta G^0'$) for HT between organic hydrides and CO_2 in DMSO at 100°C. Experimental values are denoted with black circles, whereas calculated values are shown with red circles. Blue circles represent calculated values for HT to water (HER). Solid lines correspond to fits to the Marcus model. Reproduced with permission from ref 3. Copyright 2021 American Chemical Society.

To illustrate what these self-exchange values mean for the catalytic HT, we evaluated HT rates for a hypothetical electrocatalyst for CO_2 reduction to formate that operates via outer-sphere hydride transfer in the DMSO solvent at room temperature and at the driving force of -0.1 eV (Table 1). Under these conditions, we found that the HT from organic hydride donor catalysts to CO_2 would occur at a rate of $2.5 \cdot 10^{-6} M^{-1}s^{-1}$, which is prohibitively slow. If organic hydride donor catalysts were replaced with metal-based hydride donors, such as $[Ru(trpy)(bpy)H]^+$, the HT rate would improve significantly to $8 \cdot 10^{-3} M^{-1}s^{-1}$. This finding shows that the metal-based hydride donors are expected to be kinetically much more efficient than the corresponding organic analogs. However, even with metal-based catalysts, the HT reaction is still quite slow, which explains why formate formation is less commonly observed as a product during homogeneous CO_2 reduction electrocatalysis. Our analysis also predicts the maximum rate for HT to CO_2 , which involves a

hypothetical hydride donor with self-exchange reorganization energy $\lambda_{RH} = 0$ kcal/mol. The value of $3 \cdot 10^3$ M⁻¹s⁻¹ is many orders of magnitude better than that obtained for metal-free and metal-based hydrides. However, this is still barely sufficient to enable catalytic rates greater than 100 turnovers per second, which is required to keep up with the photon flux of solar irradiance. Nonetheless, it should be emphasized that the kinetic analysis shown here applies systems that exclusively undergo outer-sphere hydride transfers and in the DMSO solvent. Other mechanisms, such as CO₂ insertion into the hydride bond,⁶⁷ and different solvent systems may contribute to higher catalytic activities, as witnessed by reports on several CO₂-to-formate metal-based catalysts.

Table 1: Summary of self-exchange reorganization energies and estimated HT rate constants for a metal-free, metal-based, and an ideal hydride donor for CO₂ reduction that operates at 25°C with -0.1 eV thermodynamic driving force, in the DMSO solvent. Reproduced with permission from ref 3. Copyright 2021 American Chemical Society.

Hydride donor	λ_{RH} (kcal/mol)	λ (kcal/mol)	k_{HT} (M ⁻¹ s ⁻¹)
NADH analogue	98.4	74.0	2.5×10^{-6}
[Ru(trpy)(bpy)H] ⁺	60.0	54.6	8.0×10^{-3}
Ideal	0	24.6	3.0×10^3

Hydride Regeneration

Electrochemical Regeneration. Organic hydride donors have been extensively used as stoichiometric reducing reagents in many organic HT transformations. However, their use as catalysts has been limited due to the difficulties associated with hydride regeneration. First, the electrochemical regeneration of organic hydrides from R⁺ derivatives is hampered by the tendency of one-electron reduced R[•] radicals to dimerize.^{4,54,68} The dimer formation is irreversible, leading to the deactivation of the catalyst. We found that the dimerization rate can be reduced by the introduction of bulky substituents. For example, functionalization at the 2-position of benzimidazolium derivatives with bulky substituents, such as a mesityl group or a (1,3,5)-trimethoxybenzene group, stabilized the radical form. This was evidenced by their CV, which illustrated a reversible couple for the first reduction of the BIM⁺ derivatives.⁴ In addition, the functionalization in the 2-position also imparted additional driving force for HT from BIMH due to additional R⁺ stabilization, relative to the unfunctionalized HBIMH.³

The second challenge is associated with exceptionally negative standard reduction potentials for the R[•]/R⁻ couple. To exemplify this, Figure 6 compares the regeneration energy landscape for one of our organic hydride, 2OH, with the corresponding energy landscape for the Ni-based hydride donor that exhibits an essentially identical hydricity. The first reduction steps, namely R⁺/R[•], for the organic analog and the Ni²⁺/Ni⁺ couple for the metal-based derivative, occur with similar standard reduction potentials (~-0.5 V vs NHE). However, the energy requirements for the second reduction step (R[•]/R⁻ and Ni⁺/Ni⁰) are significantly different: organic hydrides require a potential

of -1.4 V vs NHE, while the metal-based system undergoes second reduction step at only -0.5 V vs NHE. Such differences in the energy landscapes clearly point to the ability of d-orbitals on metal centers to accumulate multiple charges at relatively modest potentials, while metal-free p-orbitals cannot screen the accumulated charges as efficiently. Thus, an efficient approach toward regeneration of metal-free hydrides must avoid the formation of high-energy R^- intermediates, which can in principle be achieved using PCET (Figure 6). Specifically, if pKa values of RH^+ and the proton source are selected to enable the protonation of R^* , the subsequent reduction step involving the RH^+/RH couple is expected to occur at more positive potentials. Such PCET mechanisms are often utilized in natural and artificial catalysis and are an excellent method to minimize energy penalties associated with the formation of charged intermediates.

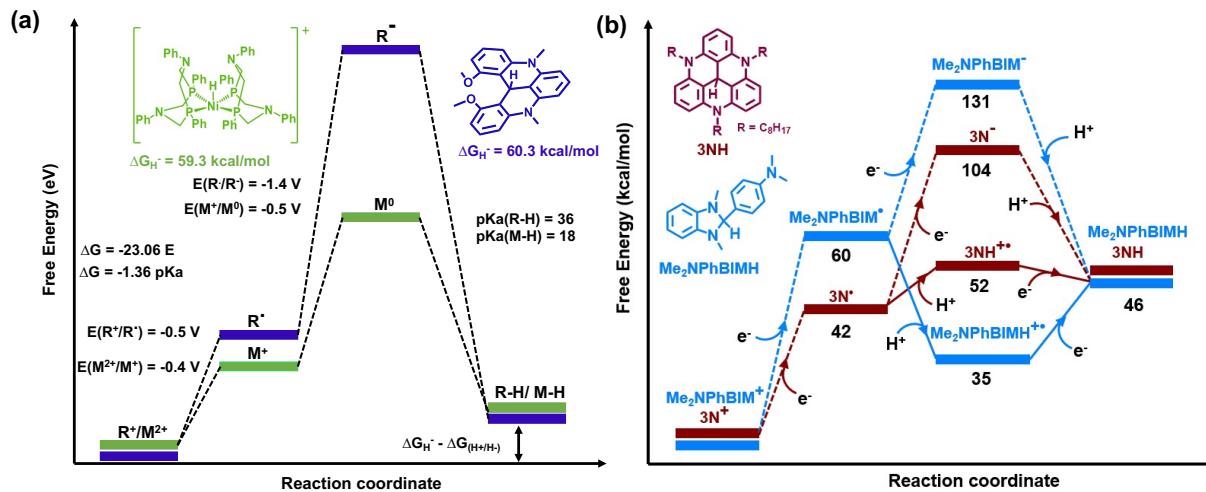


Figure 6. The comparison of the energy diagram profiles for (a) the regeneration of a metal-based hydride ($[\text{Ni}(\text{P}^{\text{Ph}}_2\text{N}^{\text{Ph}})_2\text{H}]^+$) (green color) and metal-free hydride (2OH) (blue color) in acetonitrile, (b) the regeneration via electron-electron-proton (dotted line) and electron-proton-electron sequences (solid line) for benzimidazole-based (blue) and acridine-based hydrides (brown) in DMSO. Reproduced with permission from ref 1 and 4. Copyright 2018 American Chemical Society and 2019 Royal Society of Chemistry.

To pinpoint the conditions needed to perform PCET during the regeneration of our organic hydrides, we computationally evaluated the pKa values of our RH^+ intermediates (Figure 7).⁴ We found that the pKa values of acridine-based hydrides tend to be very low, in the range from -6.4 to $+1.7$ in DMSO. These values indicate that the PCET mechanism with acridine-based derivatives can operate only under extremely acidic conditions, which are impractical for electrocatalysis. However, the situation was different for benzimidazole-based derivatives, where $\text{pK}_a(\text{RH}^+)$ values are in the 12.4 – 21.4 range. Higher pKa values of benzimidazole derivatives were explained by differences in the stability of neutral R^* radicals: cyclopentyl radicals in benzimidazoles are destabilized by the ring strain, even more so than the corresponding ring strain destabilization associated with cyclohexyl radicals in acridines. These acidity constants indicate that the efficient protonation of benzimidazole-based R^* intermediates can be achieved under mild conditions, using weak acids. Once protonated, the RH^+ are easily reduced, with standard reduction potentials moving to the $E^\circ(\text{RH}^+/\text{RH}) = -0.34$ to $+0.19$ V vs. NHE range. Such positive shift in the second

reduction step changes the potential-liming process to the first reduction process associated with the R^+/R^\bullet couple. Thus, the negative effects associated with the high-energy R^- intermediates can be efficiently circumvented in the case of benzimidazole-based hydrides.

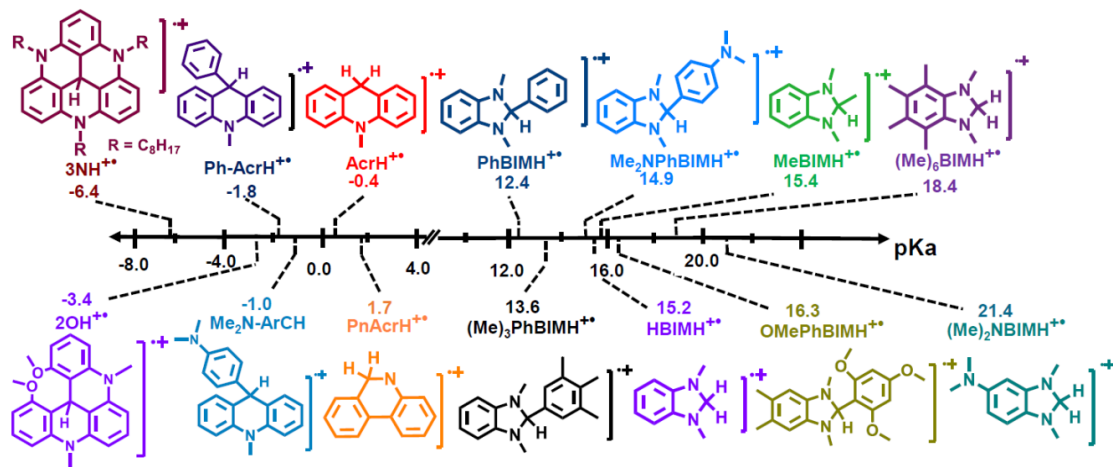


Figure 7. pKa values for the radical-cation forms of acridine- and benzimidazole- model compounds in DMSO. Values obtained from DFT calculations at the wB97XD/6-311+G(d,p) level of theory. Data taken from ref. ⁴

The significance of these theoretical predictions was tested using the benzimidazole $Me_2NPhBIM^+$.⁴ Cyclic voltammogram of $Me_2NPhBIM^+$ (Figure 8A) showed that the first reduction step, associated with the R^+/R^\bullet couple, is chemically irreversible and this behavior has been assigned to the radical dimerization process, which was confirmed by the appearance of the dimer oxidation peak at -0.84 V vs. Fc/Fc^+ (-0.21 V vs. NHE) in the return sweep. In the presence of acetic acid as a proton source, the dimerization process is suppressed, which can be observed as the disappearance of the dimer oxidation peak in the anodic sweep. Instead, the PCET mechanism takes place, leading to the formation of the hydride form, $Me_2NPhBIMH$, evidenced by the appearance of the hydride oxidation peak at -0.34 V vs. Fc/Fc^+ ($+0.29$ V vs. NHE). The overall effect of the PCET mechanism is notable: it not only suppresses the unwanted radical dimerization process, but it also lowers the energy requirements for the hydride regeneration. We further demonstrated that the regeneration of benzimidazole hydrides can be achieved efficiently using controlled-potential electrolysis, where the NMR spectra of catholyte before and after electrolysis illustrates quantitative conversion from cation to the hydride form (Figure 8B).

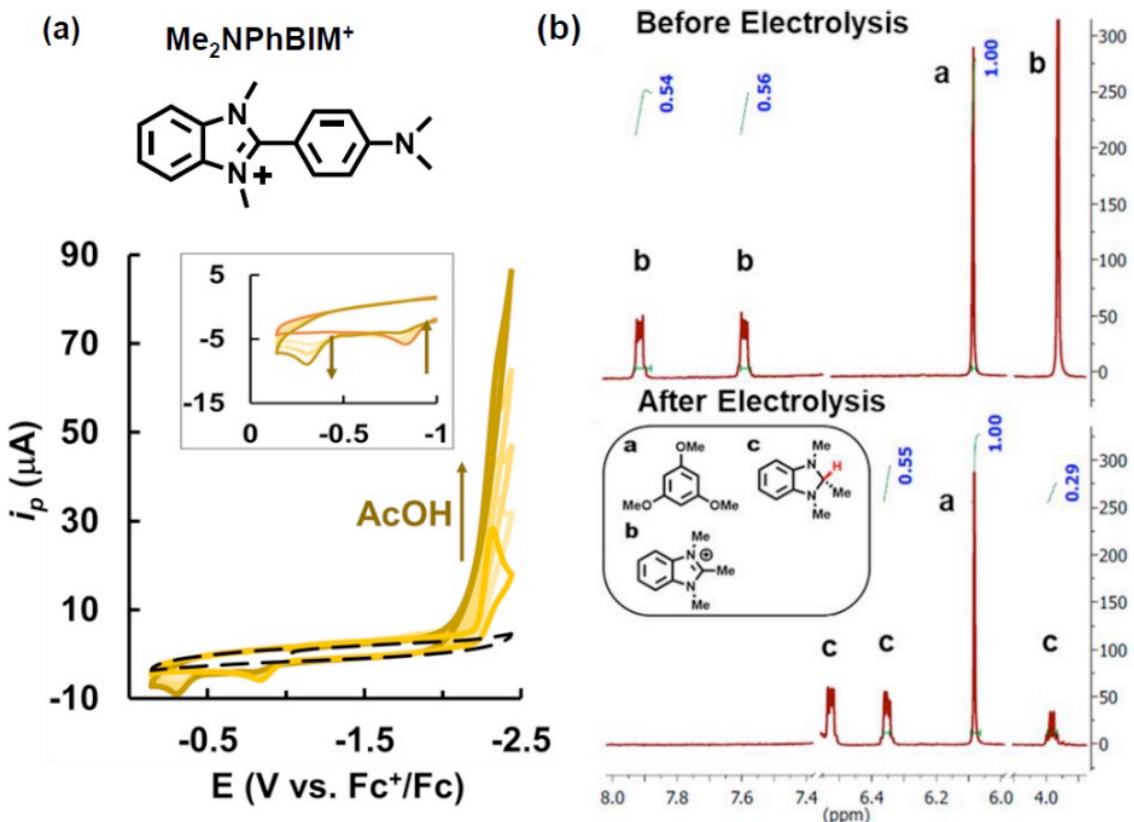


Figure 8. (a) Cyclic voltammograms of $\text{Me}_2\text{NPhBIM}^+$ in the presence of AcOH in DMSO. (b) ^1H NMR spectra of catholyte solution before and after electrolysis, in DMSO-d_6 . Reproduced with permission from ref 4 and 2, respectively. Copyright 2019 Royal Society of Chemistry and 2019 American Chemical Society.

Photochemical Regeneration. Apart from the electrochemical regeneration, organic hydride donors can also be regenerated photochemically analogously to natural photosynthesis. In this approach, the light is absorbed by a semiconductor to generate electrons needed for the hydride formation. The photochemical approach of organic hydride donors is appealing because it combines the use of a renewable solar energy source with solar fuel production. In our previous work, we explored the photochemical regeneration of organic hydrides by contacting the corresponding hydride acceptors R^+ to p-type mid- and wide-gap inorganic semiconductors, GaP and NiO. In these studies, the light harvesting was achieved either by the organic moiety (R^+ or R^\bullet) or by the semiconductor (GaP), while the regeneration mechanisms were explored using time-resolved laser spectroscopy. To avoid challenges associated with dimerization of neutral radical R^\bullet species, the photochemical studies were performed using organic hydride donors that produce stable radicals.

In our initial work, we explored light-induced electron transfer from p-GaP to physisorbed triarylmethane, flavin and acridine R^+ derivatives (Figure 9a). The R^+/GaP system represents a dual light-harvesting assembly: the blue photons can be absorbed by GaP, while red photons can be absorbed by R^+ . Thus, the R^+ derivatives were chosen based on their ability to absorb the light above 550 nm (absorption cutoff for p-GaP) and their capability to inject holes into p-GaP upon

photoexcitation. Indeed, all dyes exhibited favorable thermodynamic characteristics for photo-induced electron transfer from p-GaP, as determined using their UV-Vis absorption spectra and cyclic voltammograms.⁶⁹ The photochemical reduction of R^+ derivatives to the corresponding neutral R^\bullet derivatives was achieved efficiently for photoexcitation of GaP, as illustrated by the current increase at wavelengths shorter than 550 nm (Figure 9b). However, despite favorable thermodynamics, the photoelectrochemical measurements illustrated successful sub-bandgap sensitization for only $2O^+$ and $Et\text{-FI}^+$, as represented with the rise in photocurrent above 550 nm (Figure 9a). The lack of sub-gap photocurrent in other dyes was explained by their short-lived excited state lifetimes and confirmed by the detection of short-lived transients in pump-probe spectroscopy measurements of these dyes in solution (Figure 9c). Thus, the dual light-harvesting mechanism explored in this study works well, if the excited-state lifetime of R^+ analogs exceed several hundreds of picoseconds. Overall, this study illustrated that the first electron reduction of R^+ analogs can be efficiently achieved using photoactive p-type semiconductors.

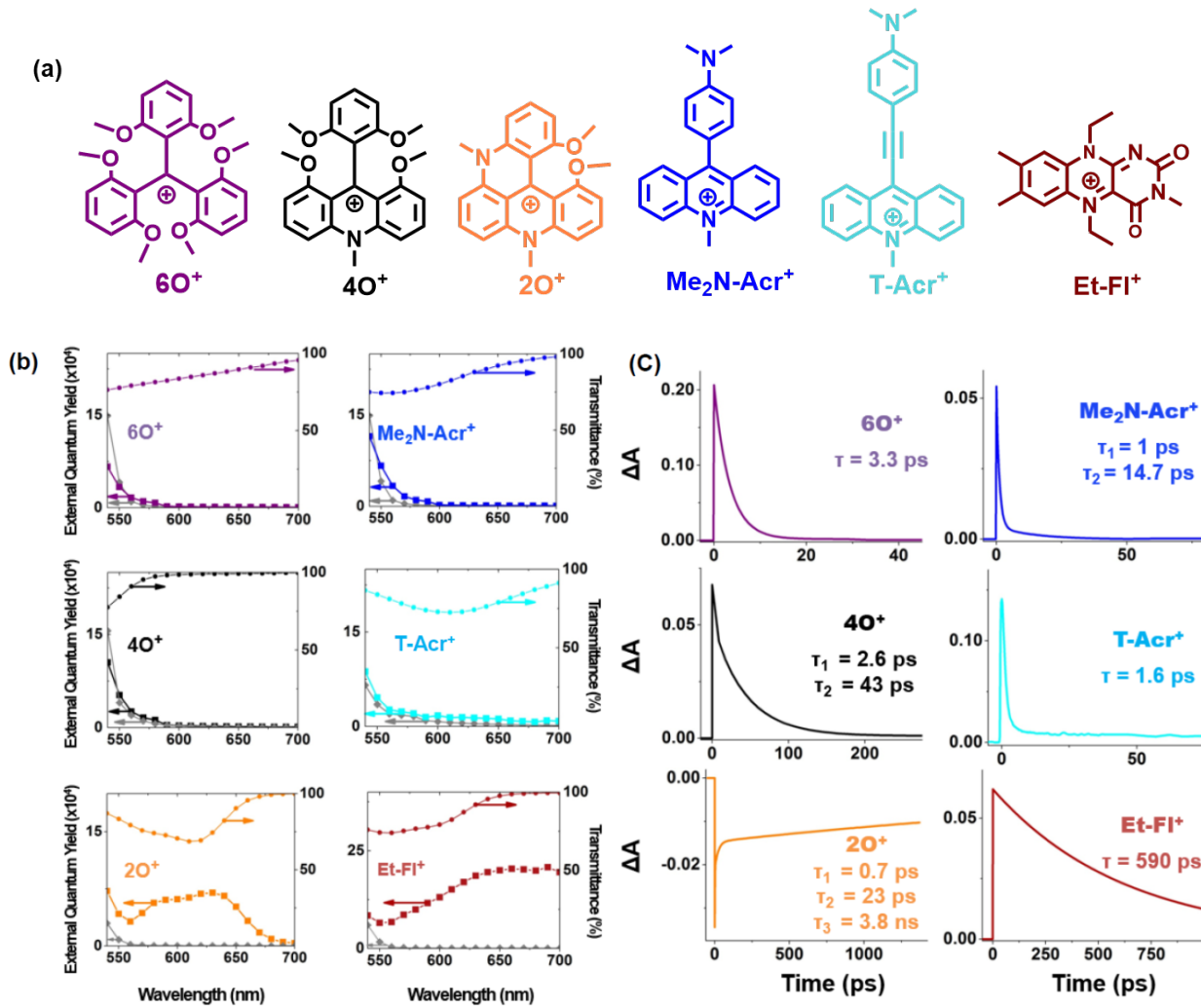
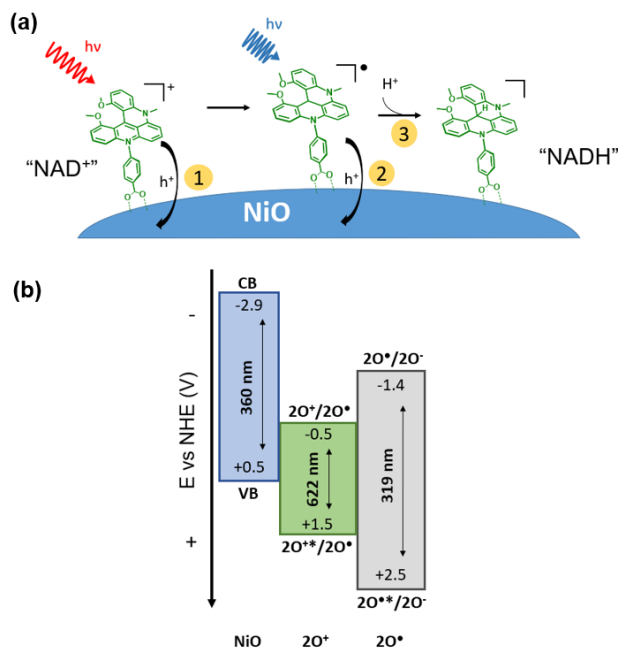


Figure 9. Photoreduction of R^+ /GaP dual absorber system: (a) structures of R^+ . (b) Photocurrent response measurements of p-GaP sensitized in the presence (colored squares) and absence (gray diamonds) of R^+ derivatives. Colored circles represent the transmittance of the corresponding R^+

derivatives in solution. (c) Kinetic transient absorption traces of model compounds in acetonitrile. Reproduced with permission from ref 69. Copyright 2016 American Chemical Society.

In the follow-up study, we explored the dye-sensitization approach as a mechanism of performing the two-electron reduction of R^+ , to enable the regeneration of organic hydride donors.^{1,53} Unfortunately, a complete regeneration could not be achieved using p-GaP, since its valence band edge energy does not provide sufficient driving force for the second electron reduction of most R^+ derivatives. To circumvent this challenge, we instead explored the use of a wide-gap semiconductor, p-NiO. The valence band energy of p-NiO enables hole injections from photoexcited R^+ and R^\bullet radical species (Scheme 3b). Each photoreduction step was studied using femtosecond transient absorption on the synthesized $2\text{O}^+@\text{p-NiO}$ and $2\text{O}^\bullet@\text{p-NiO}$ composites. While the obtained time-resolved data point towards feasible photochemical conversion of 2O^+ to the corresponding hydride 2OH with the multiple-electron accumulation approach, several drawbacks remain to be addressed. First, the $2\text{O}^+@\text{p-NiO}$ composite exhibits a rapid charge recombination: much of the charge-separated population recombines within 40 ps, caused in part by the poor electrical conductivity of p-NiO. Furthermore, the absorption of the $2\text{O}^\bullet@\text{p-NiO}$ composite in the visible range is low, making it an inefficient harvester of solar radiation. Future studies should focus on the design of NAD^+ analogs that can achieve the long-distance charge-separation and that can produce radicals with favorable absorption properties in the visible range.

Scheme 3. (a) Schematic representation of the multi-electron accumulation approach used for the photochemical reduction of 2O^+ to 2OH . (b) Energy diagram showing the band edge potentials for NiO, ground and excited-state reduction potentials of 2O^+ and 2O^\bullet . Reproduced with permission from ref 5. Copyright 2019 American Chemical Society.



Conclusions and Outlook

Our discoveries of efficient hydride transfer to CO_2 and successful regeneration of hydride donors using proton-coupled mechanisms represent important steps towards organocatalytic reduction processes. However, despite the tremendous effort and significant advances in recent years, several outstanding challenges need to be addressed before the metal-free catalytic system is realized. First, our studies indicate that the HT kinetics are sluggish. To enable room-temperature catalysis, hydride donors with low $\text{R-H}/\text{R}^+$ self-exchange reorganization energies need to be discovered. One possible way this can be achieved is by minimizing the structural change that occurs as the hydride form, where the sp^3 carbon center is converted into the cation form containing planar sp^2 carbocation. The second challenge is associated with the large overpotential associated with the catalytic reduction of CO_2 to formate by organic (and metal-based) hydrides. Finding creative ways to circumvent the scaling relationships shown in Figure 3 will be essential for the discovery of fast and selective CO_2 reduction catalysts. An interesting method where this can be achieved has been put forward by Yang and co-authors,²⁶ who point out that HT in enzymatic $\text{CO}_2/\text{HCOO}^-$ conversion involves a bidirectional mechanism with electron and proton transfer steps occurring from separate moieties of the catalyst. Discovery of biomimetic catalysts with similar behavior can lead to efficient lowering of the reaction overpotential, since the pK_a value of the proton source and the standard reduction potential of the electron source can be independently tuned to achieve ideal thermodynamic conditions for catalysis.

Once these challenges are addressed, metal-free HT catalysts are expected to serve as excellent alternatives for their metal-based counterparts. The most obvious advantages of using metal-free hydrides are that they are composed of earth-abundant elements and that they do not impose a threat to the environment. In addition, the CO_2 reduction by organic hydride donors proceeds with high selectivity, due to the HT mechanism: since none of the intermediates: R^+ , R^{\cdot} and R-H show appreciable binding interaction towards CO_2 , the formation of CO does not occur. This reactivity can be explored to enable the sequence of HT steps, starting with the reduction of CO_2 to formate, followed by the reduction of formate to formaldehyde, and ending with the reduction of formaldehyde to methanol. Overall, this proton-coupled six-electron reduction of CO_2 to methanol, if catalyzed by inexpensive organocatalysts, represents an appealing approach toward large-scale CO_2 upcycling using renewable energy sources.

Author Information

Corresponding Author email: glusac@uic.edu

ORCID:

Stefan Ilic, <http://orcid.org/0000-0002-6305-4001>

Ksenija D. Glusac, <http://orcid.org/0000-0002-2734-057X>

Biographies

Stefan Ilic obtained his Ph.D. at University of Illinois Chicago in 2019 and then conducted his postdoctoral research at Virginia Tech, mentored by Prof. Amanda J. Morris. He is currently working at Argonne National Laboratory as a postdoctoral appointee in the JCESR hub. His research interests focus on clean energy conversion and storage systems.

Jonathan L Gesiorski obtained his M.Sc. at University of Illinois Chicago in 2021. His research in the Glusac group focused on biomimetic NADH analog catalysts.

Ravindra B Weerasooriya obtained his Ph.D. at University of Illinois Chicago in 2021. His research in the Glusac group focused on biomimetic NADH analog catalysts.

Ksenija D. Glusac obtained her Ph.D. at University of Florida and then completed postdoctoral training at Standford University. She started her independent academic career at Bowling Green State University, where she spent 10 years. She is currently a Professor of Chemistry at University of Illinois Chicago with a joint appointment at Argonne National Laboratory. Her research is focused on carbon-based motifs in photo- and electro-catalysts relevant to energy storage and solar fuel applications.

Acknowledgments

Ongoing research is supported by the National Science Foundation under award 1954298.

References

- (1) Ilic, S.; Pandey Kadel, U.; Basdogan, Y.; Keith, J. A.; Glusac, K. D. Thermodynamic Hydricities of Biomimetic Organic Hydride Donors. *Journal of the American Chemical Society* **2018**, *140*, 4569–4579. <https://doi.org/10.1021/jacs.7b13526>.
- (2) Lim, C.-H.; Ilic, S.; Alherz, A.; Worrell, B. T.; Bacon, S. S.; Hynes, J. T.; Glusac, K. D.; Musgrave, C. B. Benzimidazoles as Metal-Free and Recyclable Hydrides for CO₂ Reduction to Formate. *Journal of the American Chemical Society* **2019**, *141*, 272–280. <https://doi.org/10.1021/jacs.8b09653>.
- (3) Weerasooriya, R. B.; Gesiorski, J. L.; Alherz, A.; Ilic, S.; Hargenrader, G. N.; Musgrave, C. B.; Glusac, K. D. Kinetics of Hydride Transfer from Catalytic Metal-Free Hydride Donors to CO₂. *The Journal of Physical Chemistry Letters* **2021**, *12*, 2306–2311. <https://doi.org/10.1021/acs.jpcllett.0c03662>.
- (4) Ilic, S.; Alherz, A.; Musgrave, C. B.; Glusac, K. D. Importance of Proton-Coupled Electron Transfer in Cathodic Regeneration of Organic Hydrides. *Chemical Communications* **2019**, *55*, 5583–5586. <https://doi.org/https://doi.org/10.1039/C9CC00928K>.
- (5) Hepburn, C.; Adlen, E.; Beddington, J.; Carter, E. A.; Fuss, S.; Mac Dowell, N.; Minx, J. C.; Smith, P.; Williams, C. K. The Technological and Economic Prospects for CO₂ Utilization and Removal. *Nature* **2019**, *575*, 87–97. <https://doi.org/10.1038/s41586-019-1681-6>.
- (6) Aresta, M.; Dibenedetto, A.; Angelini, A. Catalysis for the Valorization of Exhaust Carbon: From CO₂ to Chemicals, Materials, and Fuels. Technological Use of CO₂. *Chemical Reviews* **2014**, *114*, 1709–1742. <https://doi.org/10.1021/cr4002758>.
- (7) Parsons Brinckerhoff. *ACCELERATING THE UPTAKE OF CCS: INDUSTRIAL USE OF CAPTURED CARBON DIOXIDE*; 2011.
- (8) Peter, S. C. Reduction of CO₂ to Chemicals and Fuels: A Solution to Global Warming and Energy Crisis. *ACS Energy Letters* **2018**, *3*, 1557–1561. <https://doi.org/10.1021/acsenergylett.8b00878>.
- (9) Hassanzadeh, H.; Mansouri, S. H. Efficiency of Ideal Fuel Cell and Carnot Cycle from a Fundamental Perspective. *Proceedings of the Institution of Mechanical Engineers, Part A*:

Journal of Power and Energy **2005**, *219*, 245–254.
<https://doi.org/10.1243/095765005X28571>.

(10) Francke, R.; Schille, B.; Roemelt, M. Homogeneously Catalyzed Electroreduction of Carbon Dioxide—Methods, Mechanisms, and Catalysts. *Chemical Reviews* **2018**, *118*, 4631–4701. <https://doi.org/10.1021/acs.chemrev.7b00459>.

(11) Elouarzaki, K.; Kannan, V.; Jose, V.; Sabharwal, H. S.; Lee, J.-M. Recent Trends, Benchmarking, and Challenges of Electrochemical Reduction of CO₂ by Molecular Catalysts. *Advanced Energy Materials* **2019**, *9*, 1900090.
<https://doi.org/https://doi.org/10.1002/aenm.201900090>.

(12) Costentin, C.; Robert, M.; Savéant, J.-M. Catalysis of the Electrochemical Reduction of Carbon Dioxide. *Chemical Society Reviews* **2013**, *42*, 2423–2436.
<https://doi.org/10.1039/C2CS35360A>.

(13) Barlow, J. M.; Yang, J. Y. Thermodynamic Considerations for Optimizing Selective CO₂ Reduction by Molecular Catalysts. *ACS Central Science* **2019**, *5*, 580–588.
<https://doi.org/10.1021/acscentsci.9b00095>.

(14) Saouma, C. T.; Day, M. W.; Peters, J. C. CO₂ Reduction by Fe(i): Solvent Control of C–O Cleavage versus C–C Coupling. *Chemical Science* **2013**, *4*, 4042–4051
<https://doi.org/10.1039/c3sc51262b>.

(15) Savéant, J.-M. Molecular Catalysis of Electrochemical Reactions. Mechanistic Aspects. *Chemical Reviews* **2008**, *108*, 2348–2378. <https://doi.org/10.1021/cr068079z>.

(16) Elgrishi, N.; Chambers, M. B.; Artero, V.; Fontecave, M. Terpyridine Complexes of First Row Transition Metals and Electrochemical Reduction of CO₂ to CO. *Physical Chemistry Chemical Physics* **2014**, *16*, 13635–13644. <https://doi.org/10.1039/C4CP00451E>.

(17) Elgrishi, N.; Chambers, M. B.; Fontecave, M. Turning It off! Disfavouring Hydrogen Evolution to Enhance Selectivity for CO Production during Homogeneous CO₂ Reduction by Cobalt–Terpyridine Complexes. *Chemical Science* **2015**, *6*, 2522–2531.
<https://doi.org/10.1039/C4SC03766A>.

(18) Zhanaidarova, A.; Jones, S. C.; Despagnet-Ayoub, E.; Pimentel, B. R.; Kubiak, C. P. Re(TBu-Bpy)(CO)₃Cl Supported on Multi-Walled Carbon Nanotubes Selectively Reduces CO₂ in Water. *Journal of the American Chemical Society* **2019**, *141*, 17270–17277. <https://doi.org/10.1021/jacs.9b08445>.

(19) Chen, Z.; Chen, C.; Weinberg, D. R.; Kang, P.; Concepcion, J. J.; Harrison, D. P.; Brookhart, M. S.; Meyer, T. J. Electrocatalytic Reduction of CO₂ to CO by Polypyridyl Ruthenium Complexes. *Chemical Communications* **2011**, *47*, 12607–12609.
<https://doi.org/10.1039/C1CC15071E>.

(20) Chen, Z.; Kang, P.; Zhang, M.-T.; Meyer, T. J. Making Syngas Electrocatalytically Using a Polypyridyl Ruthenium Catalyst. *Chemical Communications* **2014**, *50*, 335–337.
<https://doi.org/10.1039/C3CC47251E>.

(21) Woolerton, T. W.; Sheard, S.; Reisner, E.; Pierce, E.; Ragsdale, S. W.; Armstrong, F. A. Efficient and Clean Photoreduction of CO₂ to CO by Enzyme-Modified TiO₂ Nanoparticles Using Visible Light. *Journal of the American Chemical Society* **2010**, *132*, 2132–2133. <https://doi.org/10.1021/ja910091z>.

(22) Kuehnel, M. F.; Orchard, K. L.; Dalle, K. E.; Reisner, E. Selective Photocatalytic CO₂ Reduction in Water through Anchoring of a Molecular Ni Catalyst on CdS Nanocrystals. *Journal of the American Chemical Society* **2017**, *139*, 7217–7223.
<https://doi.org/10.1021/jacs.7b00369>.

(23) Wiedner, E. S.; Chambers, M. B.; Pitman, C. L.; Bullock, R. M.; Miller, A. J. M.; Appel, A. M. Thermodynamic Hydricity of Transition Metal Hydrides. *Chemical Reviews* **2016**, *116*, 8655–8692. <https://doi.org/10.1021/acs.chemrev.6b00168>.

(24) Waldie, K. M.; Ostericher, A. L.; Reineke, M. H.; Sasayama, A. F.; Kubiak, C. P. Hydricity of Transition-Metal Hydrides: Thermodynamic Considerations for CO₂ Reduction. *ACS Catalysis* **2018**, *8*, 1313–1324. <https://doi.org/10.1021/acscatal.7b03396>.

(25) Kinzel, N. W.; Werlé, C.; Leitner, W. Transition Metal Complexes as Catalysts for the Electroconversion of CO₂: An Organometallic Perspective. *Angewandte Chemie International Edition* **2021**, *60*, 11628–11686. <https://doi.org/https://doi.org/10.1002/anie.202006988>.

(26) Yang, J. Y.; Kerr, T. A.; Wang, X. S.; Barlow, J. M. Reducing CO₂ to HCO₂– at Mild Potentials: Lessons from Formate Dehydrogenase. *Journal of the American Chemical Society* **2020**, *142*, 19438–19445. <https://doi.org/10.1021/jacs.0c07965>.

(27) Cunningham, D. W.; Barlow, J. M.; Velazquez, R. S.; Yang, J. Y. Reversible and Selective CO₂ to HCO₂– Electrocatalysis near the Thermodynamic Potential. *Angewandte Chemie International Edition* **2020**, *59*, 4443–4447. <https://doi.org/https://doi.org/10.1002/anie.201913198>.

(28) Ceballos, B. M.; Yang, J. Y. Highly Selective Electrocatalytic CO₂ Reduction by [Pt(Dmpe)2]2+ through Kinetic and Thermodynamic Control. *Organometallics* **2020**, *39*, 1491–1496. <https://doi.org/10.1021/acs.organomet.9b00720>.

(29) Boston, D. J.; Pachón, Y. M. F.; Lezna, R. O.; de Tacconi, N. R.; MacDonnell, F. M. Electrocatalytic and Photocatalytic Conversion of CO₂ to Methanol Using Ruthenium Complexes with Internal Pyridyl Cocatalysts. *Inorganic Chemistry* **2014**, *53*, 6544–6553. <https://doi.org/10.1021/ic500051m>.

(30) Bi, J.; Hou, P.; Liu, F.-W.; Kang, P. Electrocatalytic Reduction of CO₂ to Methanol by Iron Tetradeятate Phosphine Complex Through Amidation Strategy. *ChemSusChem* **2019**, *12*, 2195–2201. <https://doi.org/https://doi.org/10.1002/cssc.201802929>.

(31) Wiedner, E. S.; Chambers, M. B.; Pitman, C. L.; Bullock, R. M.; Miller, A. J. M.; Appel, A. M. Thermodynamic Hydricity of Transition Metal Hydrides. *Chemical Reviews* **2016**, *116*, 8655–8692. <https://doi.org/10.1021/acs.chemrev.6b00168>.

(32) Taheri, A.; Thompson, E. J.; Fettinger, J. C.; Berben, L. A. An Iron Electrocatalyst for Selective Reduction of CO₂ to Formate in Water: Including Thermochemical Insights. *ACS Catalysis* **2015**, *5*, 7140–7151. <https://doi.org/10.1021/acscatal.5b01708>.

(33) Yang, J. Y.; Kerr, T. A.; Wang, X. S.; Barlow, J. M. Reducing CO₂ to HCO₂– at Mild Potentials: Lessons from Formate Dehydrogenase. *Journal of the American Chemical Society* **2020**, *142*, 19438–19445. <https://doi.org/10.1021/jacs.0c07965>.

(34) Bhattacharya, M.; Sebghati, S.; Vanderlinde, R. T.; Saouma, C. T. Toward Combined Carbon Capture and Recycling: Addition of an Amine Alters Product Selectivity from CO to Formic Acid in Manganese Catalyzed Reduction of CO₂. *Journal of the American Chemical Society* **2020**, *142*, 17589–17597. <https://doi.org/10.1021/jacs.0c07763>.

(35) Schneider, G.; Lindqvist, Y.; Branden, C. I. Rubisco: Structure and Mechanism. *Annual Review of Biophysics and Biomolecular Structure* **1992**, *21*, 119–143. <https://doi.org/10.1146/annurev.bb.21.060192.001003>.

(36) Olah, G. A.; Prakash, G. K. S.; Goepert, A. Anthropogenic Chemical Carbon Cycle for a Sustainable Future. *Journal of the American Chemical Society* **2011**, *133*, 12881–12898. <https://doi.org/10.1021/ja202642y>.

(37) Heiden, Z. M.; Lathem, A. P. Establishing the Hydride Donor Abilities of Main Group Hydrides. *Organometallics* **2015**, *34*, 1818–1827. <https://doi.org/10.1021/om5011512>.

(38) Tsay, C.; Livesay, B. N.; Ruelas, S.; Yang, J. Y. Solvation Effects on Transition Metal Hydricity. *Journal of the American Chemical Society* **2015**, *137*, 14114–14121. <https://doi.org/10.1021/jacs.5b07777>.

(39) Curtis, C. J.; Miedaner, A.; Ellis, W. W.; DuBois, D. L. Measurement of the Hydride Donor Abilities of $[HM(\text{Diphosphine})_2]^+$ Complexes ($M = \text{Ni, Pt}$) by Heterolytic Activation of Hydrogen. *Journal of the American Chemical Society* **2002**, *124*, 1918–1925. <https://doi.org/10.1021/ja0116829>.

(40) Raebiger, J. W.; Miedaner, A.; Curtis, C. J.; Miller, S. M.; Anderson, O. P.; DuBois, D. L. Using Ligand Bite Angles To Control the Hydricity of Palladium Diphosphine Complexes. *Journal of the American Chemical Society* **2004**, *126*, 5502–5514. <https://doi.org/10.1021/ja0395240>.

(41) Creutz, C.; Chou, M. H. Hydricities of D6 Metal Hydride Complexes in Water. *Journal of the American Chemical Society* **2009**, *131*, 2794–2795. <https://doi.org/10.1021/ja809724s>.

(42) Matsubara, Y.; Fujita, E.; Doherty, M. D.; Muckerman, J. T.; Creutz, C. Thermodynamic and Kinetic Hydricity of Ruthenium(II) Hydride Complexes. *Journal of the American Chemical Society* **2012**, *134*, 15743–15757. <https://doi.org/10.1021/ja302937q>.

(43) DuBois, D. L.; Berning, D. E. Hydricity of Transition-Metal Hydrides and Its Role in CO_2 Reduction. *Applied Organometallic Chemistry* **2000**, *14*, 860–862. [https://doi.org/https://doi.org/10.1002/1099-0739\(200012\)14:12<860::AID-AOC87>3.0.CO;2-A](https://doi.org/https://doi.org/10.1002/1099-0739(200012)14:12<860::AID-AOC87>3.0.CO;2-A).

(44) Brereton, K. R.; Smith, N. E.; Hazari, N.; Miller, A. J. M. Thermodynamic and Kinetic Hydricity of Transition Metal Hydrides. *Chemical Society Reviews* **2020**, *49*, 7929–7948. <https://doi.org/10.1039/D0CS00405G>.

(45) Handoo, K. L.; Cheng, J. P.; Parker, V. D. Hydride Affinities of Organic Radicals in Solution. A Comparison of Free Radicals and Carbenium Ions as Hydride Ion Acceptors. *Journal of the American Chemical Society* **1993**, *115*, 5067–5072. <https://doi.org/10.1021/ja00065a017>.

(46) Zhu, X.-Q.; Wang, C.-H.; Liang, H.; Cheng, J.-P. Theoretical Prediction of the Hydride Affinities of Various P- and o-Quinones in DMSO. *The Journal of Organic Chemistry* **2007**, *72*, 945–956. <https://doi.org/10.1021/jo0621928>.

(47) Cheng, J.; Handoo, K. L.; Xue, J.; Parker, V. D. Free Energy Hydride Affinities of Quinones in Dimethyl Sulfoxide Solution. *The Journal of Organic Chemistry* **1993**, *58*, 5050–5054. <https://doi.org/10.1021/jo00071a011>.

(48) Ellis, W. W.; Raebiger, J. W.; Curtis, C. J.; Bruno, J. W.; DuBois, D. L. Hydricities of BzNADH , $\text{C}_5\text{H}_5\text{Mo}(\text{PMe}_3)(\text{CO})_2\text{H}$, and $\text{C}_5\text{Me}_5\text{Mo}(\text{PMe}_3)(\text{CO})_2\text{H}$ in Acetonitrile. *Journal of the American Chemical Society* **2004**, *126*, 2738–2743. <https://doi.org/10.1021/ja038567d>.

(49) Brereton, K. R.; Jadrich, C. N.; Stratakes, B. M.; Miller, A. J. M. Thermodynamic Hydricity across Solvents: Subtle Electronic Effects and Striking Ligation Effects in Iridium Hydrides. *Organometallics* **2019**, *38*, 3104–3110. <https://doi.org/10.1021/acs.organomet.9b00278>.

(50) Mathis, C. L.; Geary, J.; Ardon, Y.; Reese, M. S.; Philliber, M. A.; Vanderlinden, R. T.; Saouma, C. T. Thermodynamic Analysis of Metal-Ligand Cooperativity of PNP Ru Complexes: Implications for CO_2 Hydrogenation to Methanol and Catalyst Inhibition.

Journal of the American Chemical Society **2019**, *141*, 14317-14328.
<https://doi.org/10.1021/jacs.9b06760>.

(51) Handoo, K. L.; Cheng, J. P.; Parker, V. D. Hydride Affinities of Organic Radicals in Solution. A Comparison of Free Radicals and Carbenium Ions as Hydride Ion Acceptors. *Journal of the American Chemical Society* **1993**, *115*, 5067-5072.
<https://doi.org/10.1021/ja00065a017>.

(52) Ilic, S.; Alherz, A.; Musgrave, C. B.; Glusac, K. D. Thermodynamic and Kinetic Hydricities of Metal-Free Hydrides. *Chemical Society Reviews* **2018**, *47*, 2809–2836.
<https://doi.org/10.1039/C7CS00171A>.

(53) Hargenrader, G. N.; Weerasooriya, R. B.; Ilic, S.; Niklas, J.; Poluektov, O. G.; Glusac, K. D. Photoregeneration of Biomimetic Nicotinamide Adenine Dinucleotide Analogues via a Dye-Sensitized Approach. *ACS Applied Energy Materials* **2019**, *2*, 80–91.
<https://doi.org/10.1021/acsaem.8b01574>.

(54) Eisner, Ulli.; Kuthan, Josef. Chemistry of Dihydropyridines. *Chemical Reviews* **1972**, *72*, 1–42. <https://doi.org/10.1021/cr60275a001>.

(55) Walsh, C. Naturally Occurring 5-Deazaflavin Coenzymes: Biological Redox Roles. *Accounts of Chemical Research* **1986**, *19*, 216–221. <https://doi.org/10.1021/ar00127a004>.

(56) Hiromoto, T.; Warkentin, E.; Moll, J.; Ermler, U.; Shima, S. The Crystal Structure of an [Fe]-Hydrogenase–Substrate Complex Reveals the Framework for H₂ Activation. *Angewandte Chemie International Edition* **2009**, *48*, 6457–6460.
<https://doi.org/https://doi.org/10.1002/anie.200902695>.

(57) Brunet, P.; Wuest, J. D. Formal Transfers of Hydride from Carbon–Hydrogen Bonds. Generation of H₂ from Orthoformamides Designed To Undergo Intramolecular Protonolyses of Activated Carbon–Hydrogen Bonds. *The Journal of Organic Chemistry* **1996**, *61*, 2020–2026. <https://doi.org/10.1021/jo951636p>.

(58) Wiberg, K. B.; Bailey, W. F.; Lambert, K. M.; Stempel, Z. D. The Anomeric Effect: It's Complicated. *The Journal of Organic Chemistry* **2018**, *83*, 5242–5255.
<https://doi.org/10.1021/acs.joc.8b00707>.

(59) Rueping, M.; Sugiono, E.; Azap, C.; Theissmann, T.; Bolte, M. Enantioselective Brønsted Acid Catalyzed Transfer Hydrogenation: Organocatalytic Reduction of Imines. *Organic Letters* **2005**, *7*, 3781–3783. <https://doi.org/10.1021/ol0515964>.

(60) Ouellet, S. G.; Walji, A. M.; Macmillan, D. W. C. Enantioselective Organocatalytic Transfer Hydrogenation Reactions Using Hantzsch Esters. *Accounts of Chemical Research* **2007**, *40*, 1327–1339. <https://doi.org/10.1021/ar7001864>.

(61) Zheng, C.; You, S.-L. Transfer Hydrogenation with Hantzsch Esters and Related Organic Hydride Donors. *Chemical Society Reviews* **2012**, *41*, 2498–2518.
<https://doi.org/10.1039/C1CS15268H>.

(62) Yang, J. W.; List, B. Catalytic Asymmetric Transfer Hydrogenation of α -Ketoesters with Hantzsch Esters. *Organic Letters* **2006**, *8*, 5653–5655. <https://doi.org/10.1021/ol0624373>.

(63) Rueping, M.; Antonchick, A. P.; Theissmann, T. A Highly Enantioselective Brønsted Acid Catalyzed Cascade Reaction: Organocatalytic Transfer Hydrogenation of Quinolines and Their Application in the Synthesis of Alkaloids. *Angewandte Chemie International Edition* **2006**, *45*, 3683–3686. <https://doi.org/https://doi.org/10.1002/anie.200600191>.

(64) Ouellet, S. G.; Tuttle, J. B.; MacMillan, D. W. C. Enantioselective Organocatalytic Hydride Reduction. *Journal of the American Chemical Society* **2005**, *127*, 32–33.
<https://doi.org/10.1021/ja043834g>.

(65) Yang, J. W.; Hechavarria Fonseca, M. T.; List, B. A Metal-Free Transfer Hydrogenation: Organocatalytic Conjugate Reduction of α,β -Unsaturated Aldehydes. *Angewandte Chemie International Edition* **2004**, *43*, 6660–6662.
<https://doi.org/https://doi.org/10.1002/anie.200461816>.

(66) Bennett, L. E.; Warlop, P. Electron Transfer to Ozone: Outer-Sphere Reactivities of the Ozone/Ozonide and Related Non-Metal Redox Couples. *Inorganic Chemistry* **1990**, *29*, 1975–1981. <https://doi.org/10.1021/ic00335a040>.

(67) Hazari, N.; Heimann, J. E. Carbon Dioxide Insertion into Group 9 and 10 Metal-Element σ Bonds. *Inorganic Chemistry* **2017**, *56*, 13655–13678.
<https://doi.org/10.1021/acs.inorgchem.7b02315>.

(68) Wu, H.; Tian, C.; Song, X.; Liu, C.; Yang, D.; Jiang, Z. Methods for the Regeneration of Nicotinamide Coenzymes. *Green Chemistry* **2013**, *15*, 1773–1789.
<https://doi.org/10.1039/C3GC37129H>.

(69) Ilic, S.; Brown, E. S.; Xie, Y.; Maldonado, S.; Glusac, K. D. Sensitization of P-GaP with Monocationic Dyes: The Effect of Dye Excited-State Lifetime on Hole Injection Efficiencies. *The Journal of Physical Chemistry C* **2016**, *120*, 3145–3155.
<https://doi.org/10.1021/acs.jpcc.5b10474>.